
The Marangoni Effect and its Applications

PHY208 COURSE PROJECT

ATHARVA BAGUL 18346
GAURI KOTIWALE 18360
NIKITA WALUNJKAR 18159
OM VAKNALLI 18376
SAUMYA JAIN 18234

Preface

We came across animal locomotion on the surface of water bodies in our class. These movements don't just rely on surface tension, but also on its gradient. The marangoni propulsion in insects where chemically induced surfactants by it create surface tension gradient due to concentration change. This in turn leads to a contractile force, which helps the insect move. This is similar to the "soap boat" we used to play with as children and the "wine tears" that help us get through our adulthood. There are a lot more practical applications of the marangoni effect, which we study in this paper with the help of theoretical results, data available from previously/already conducted experiments as well as inferences drawn from our own observations.

Contents

Preface	i
List of Figures	iv
1 Introduction	1
2 Marangoni Propulsion	2
2.1 Aim	2
2.2 Apparatus and reagents required:	2
2.3 Theory	2
2.4 Procedure	3
2.4.1 Preparation	3
2.4.2 Execution	3
2.5 Observation	5
2.6 Observation Table	5
2.7 Result	5
2.8 Precautions	5
2.9 Shortcomings	5
3 Tears of Wine	7
3.1 Introduction	7
3.2 Mechanism	8
3.3 Governing equations and formulae	8
3.3.1 Hydrodynamic Model	8
3.3.2 Finding Maximum Height of the Film (Height of the Ridge)	9
3.4 Wine Tears Experiment	11
3.4.1 Materials Used	11
3.4.2 Procedure	11
3.4.3 Expectation	11
3.4.4 Observations	11
3.4.5 Inference	13
3.4.6 Possible Errors	13
4 Microgravity and Spacecrafts	14
4.1 Introduction	14
4.2 Heat Pipes	14
4.3 CVB Experiment	14
4.4 Conclusion	17
5 Coffee Ring Effect and it's suppression	18
5.1 Introduction	18
5.2 Formation and Suppression of Coffee Rings	18
5.2.1 According to Deegan et al[1]:	18
5.2.2 According to the paper by Hua Hu and Ronald G. Larson[4]	20
5.2.3 We see the differences in the 2 papers for the following reasons :	21
5.2.4 How is Coffee ring effect suppressed in Colloids with aqueous solvent or solvents with low Marangoni flow?	22
5.3 Coffee Stain Experiment	23
5.3.1 Materials Used	23
5.3.2 Procedure	23
5.3.3 Expectation	23

5.3.4	Observation	23
5.3.5	Inference	24
5.3.6	Possible Errors	24
6	A Biological Perspective	25
6.1	Marangoni Transport in Nature	25
6.1.1	Insects walking on water	25
6.1.2	The Bond Number	26
6.1.3	Marangoni Propulsion	27
6.2	Transport of therapeutics within the lung or Marangoni enhanced pulmonary delivery strategies	27
6.2.1	The Airway Surface Liquid (ASL)	27
6.2.2	Pulmonary surfactant	28
6.2.3	Pulmonary diseases and problems in current therapy	28
6.2.4	System used to deliver the drug	29
6.2.5	Conclusion	29
7	Mantle Convection	30
8	Conclusion	31
9	References	32
9.1	For Marangoni Propulsion	32
9.2	For Tears of Wine	32
9.3	For Microgravity and Spacecrafts	32
9.4	For Coffee Rings and its Suppression	32
9.5	For The Biological Perspective	33
9.6	For Mantle Convection	33

List of Figures

1	Marangoni Propulsion Theory	3
2	Forward Propulsion	3
3	Boat Cutouts	4
4	Propulsion Exp Setup	4
5	Propulsion Exp Setup	4
6	Propulsion Observation	5
7	Propulsion Shortcomings	6
8	Wine Tears	7
9	Mechanism of Wine Tears	8
10	Cross-Sectional View of Wine Film	9
11	Height of Wine Film Meniscus	10
12	Wine Tear Exp Observations	12
13	Wine Tear Exp Observation Pictures	12
14	Wine Tear Exp Observation Pictures	12
15	Heat Transfer Pipe	15
16	CVB Exp Heat Pipe	15
17	Temp profile and heat transfer model	16
18	Interferometric images of the vapor-liquid distribution inside the same heat pipe	17
19	Coffee Stains	18
20	Evaporation with Pinned Contact Line	19
21	Increment of Evaporation in Cross Section	19
22	Quantities that determine Flow	20
23	Structure of Drop	21
24	Marangoni Flow in a Drop	22
25	Coffee Stain Experiment	24
26	Classification of Water Walkers	26
27	Marangoni Propulsion	27
28	ASL Mechanism	28

1 Introduction

The Marangoni Effect, also known as the Gibbs-Marangoni effect was first described in the 1860's by the Italian physicist Carlo Giuseppe Matteo Marangoni who investigated the spreading of oil drops on a water surface. He explained this behaviour as the macroscopic manifestation of a liquid flow as a result of local differences (gradients) in inter-facial tension. First observed by Thomson in 1855 in "Tears of Wine", J. Willard Gibbs gave a full theoretical explanation of the phenomenon in his 300 page paper "On the Equilibrium of Heterogeneous Substances" in 1875-78. This effect takes place when there is a gradient in surface tension at the surface of a liquid, generally at a gas-liquid interface. This gradient can be caused by concentration gradients or temperature gradients on the surface. As the surface tension along the interface changes, the portion of the liquid surface with higher surface tension pulls on its surrounding liquid (of lower surface tension) more strongly. This results in a contractile force and hence a mass-transfer takes place along the surface of the liquid.

This seemingly simple phenomenon results in some of the most interesting and intriguing observations, some of which are of great practical importance as well as those that pose problems in the otherwise normal functioning of devices and obstruct useful situations.

2 Marangoni Propulsion

In order to gain insights into the mechanisms of Marangoni flow, our group has preliminarily performed an experimental evidence of the said phenomenon. Below is the summary of the experiment.

2.1 Aim

To superficially analyse the Marangoni effect and experimentally quantify some parameters related to it (such as marangoni displacement and time taken).

2.2 Apparatus and reagents required:

- 2x 1-metre metal line gauges
- Cardboard
- Inch-long headed steel nails
- Thread
- Flat rectangular table tray
- Aluminium Foil
- Small soap-inert containers
- General Stationary (scissors, cutter, glue, ball-pen, adhesive tape, etc)
- Water
- Dettol “Original Liquid Handwash”
- Camphor
- High definition recording device
- Stopwatch

2.3 Theory

Surface tension gradients can serve as transport mediums due to majorly 2 causes:

- The forces created due to surface tension act along the contact lines. This is justified by Newton's 2nd law, which states that all net, unbalanced surface tension forces will lead to an acceleration in the body. Examples of this mode of transport can be seen in the interaction of solute (liquid) droplets either travelling onto the solvent surface or reacting with the solvent surface thereby self-creating the asymmetries in the surface energy gradients.
- The gradients are caused due to Marangoni flows. As it is known that surface tension gradients are usually in equilibrium with non-normal viscous forces, any disruption in the gradient will produce disequilibrated tangential stresses which would eventually lead to a flow. Familiar examples of the Marangoni transport involve any kinds of motions which include thermal gradients and/or internal introduction of surfactants.

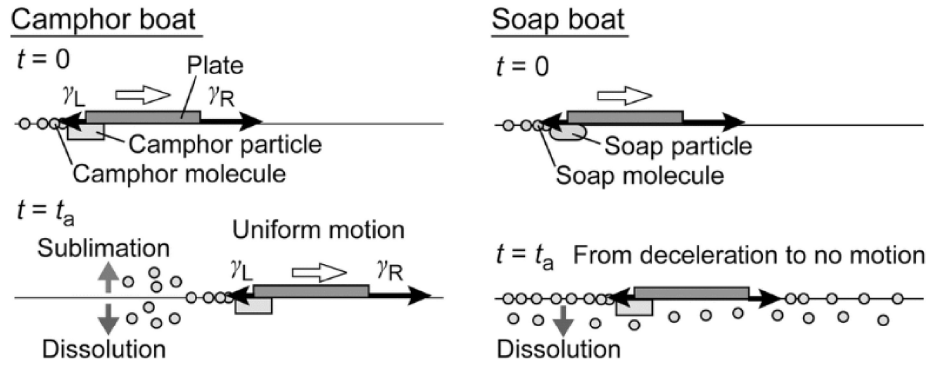


Figure 1: Camphor and Soap Boat

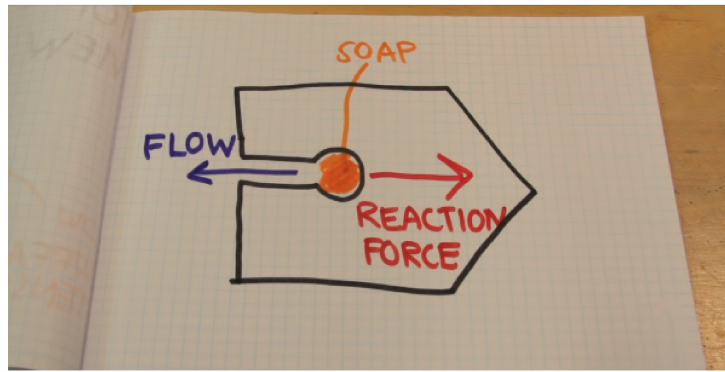


Figure 2: Propelling the Boat forward

Marangoni propulsion relates to the scenario where an asymmetric distribution of any surfactant material is generated by a body (at the surface of the liquid) which results in the disequilibrium in the surface tension as well as a Marangoni flow, whose final output is locomotion.

In this experiment, the application of the surfactant into the keyhole of the boat induces a surface-tension gradient. Since the leg of the keyhole contains a higher concentration of water (with a higher surface-tension) while the mouth contains the soap (of lower surface tension), the resultant marangoni force as well as flow occurs from the mouth towards the leg. But due to conservation of momentum, this creates an equal and opposite reaction force on the boat, thereby propelling it forward.

2.4 Procedure

2.4.1 Preparation

- Cut out the replicates of shapes as shown in the image below from the aluminium sheet. Figure 3
- With the help of the tray, scales, cardboard, thread and other stationary, built the setup shown below. Figure 4
- Made soap-water solutions with 1:1, 2:1, 3:1, 4:1 concentrations respectively. Figure 5

2.4.2 Execution

- Gently placed one of the aluminium boats onto the water surface, taking care not to submerge it.



Figure 3: Boat Cutouts

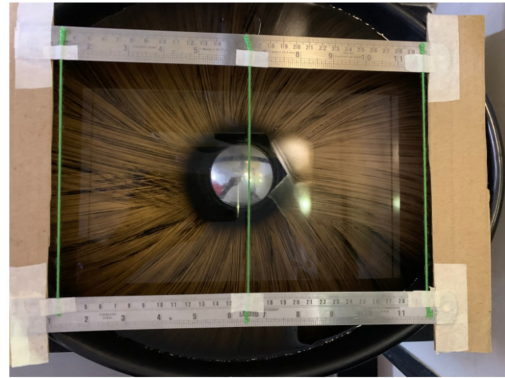


Figure 4: Exp Setup



Figure 5: Exp Setup

Solution Concentration	Initial time	Final time t2 (s)	Starting Distance	Final Distance	y2	Time Difference (t2 - Displacement)	(y2 - Average Time)	Average Time	Average Displacement
Solution 1 (1:1)	4.29	6.22	3.5	10.9		1.93	7.4	2.29	8.2
	6.11	8.75	3.5	14		2.64	10.5		
	6.02	8.33	3.5	10.2		2.31	6.7		
Solution 2 (2:1)	5.26	9.61	3.5	21.2		4.35	17.7	3.82	17.73
	5.24	8.75	3.5	19.2		3.51	15.7		
	5.75	9.35	3.5	23.3		3.6	19.8		

Figure 6: Observation Table

- Start the stopwatch.
- Dipped a nail-head into one of the soap solutions and quickly pricked the nail-head into the key-hole shape in the aluminium boat
- Recorded the propulsion onto a slow-motion video device and measured the propulsion initiation and extinction y-component displacements and time-durations.

2.5 Observation

The observation videos are attached separately. However, the 3:1 and 4:1 concentrations failed to propel the boat.

2.6 Observation Table

See Figure 6

2.7 Result

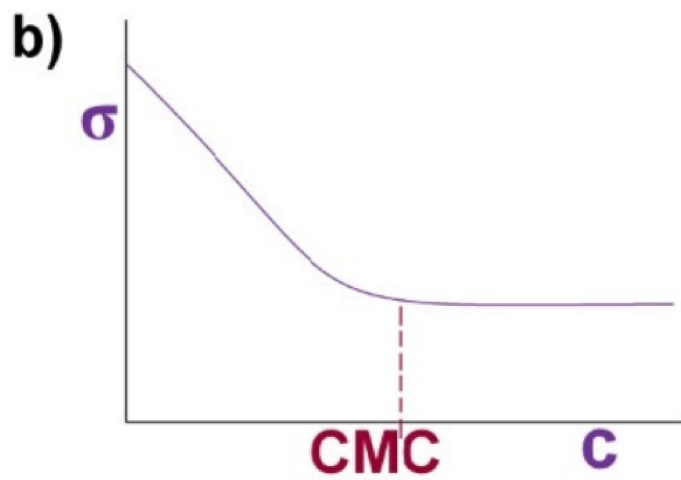
The Marangoni Propulsion was successfully observed and the average time taken and displacement were found.

2.8 Precautions

- Periodically replaced the water in the tray to avoid accumulation of the surfactant.
- Used separate set of boats, nails and containers for different surfactants to avoid contamination.
- Chose a place which has less mobility of air to avoid action of air-resistance.

2.9 Shortcomings

- Some errors were encountered due an unavoidable, minimal amount of air-flow.
- Visual and video parallax errors could have been minimised.
- More concentrated solutions can lead to micelle formations due to difference in polarity of the surfactant and the solvent. Hence the excessive concentrated solutions could have been avoided. This is one of the possible reasons that could have lead to the failure of propulsion in these samples (3:1 and 4:1).
- Determination of more complex quantities due as the instantaneous marangoni velocity and force would be difficult to compute from such an experiment.



. b) The typical dependence of σ on surfactant

Figure 7: CMC corresponds to the critical micelle concentration

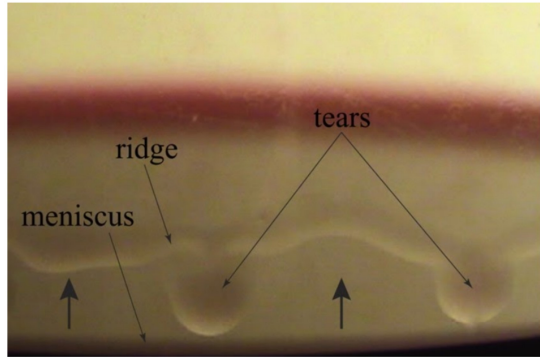


Figure 8: Thin film showing wine tears

3 Tears of Wine

Look not thou upon the wine when it is red, when it giveth his colour in the cup, when it moveth itself aright

3.1 Introduction

The phenomenon was first correctly explained by physicist James Thomson in 1855. When a wine glass is kept in open, that is without a lid, continuous formation and falling of drops of liquid along the walls of the stationary glass is observed. These drops/beads are called wine tears, wine legs, fingers, curtains, or church windows. It is most readily observed in wine of high alcohol content.

Due to marangoni stress, a thin film rises up from the meniscus and becomes thicker, forming the ridge, which is bounded on the top by an essentially stationary contact line. On this line, the three phases—glass, wine and air, coexist. Fairly regularly spaced drops form on this ridge and fall as the force of gravity overcomes the upward pull due to marangoni effect. This keeps going on till all the alcohol evaporates.

As this is a result of the concentration gradient due to the dominant effect of evaporation on the meniscus surface than the surface above the bulk, and the differential evaporation rates of water and alcohol, this effect is seen in any mixture of ethanol + water at the right conditions. As they roll down, they seem to jump back abruptly before falling back into the bulk liquid.

Temperature gradient due to evaporation and shock wave dynamics also play an important role in understanding the behaviour of these tears. However, in this paper we focus principally on their formation due to concentration change.

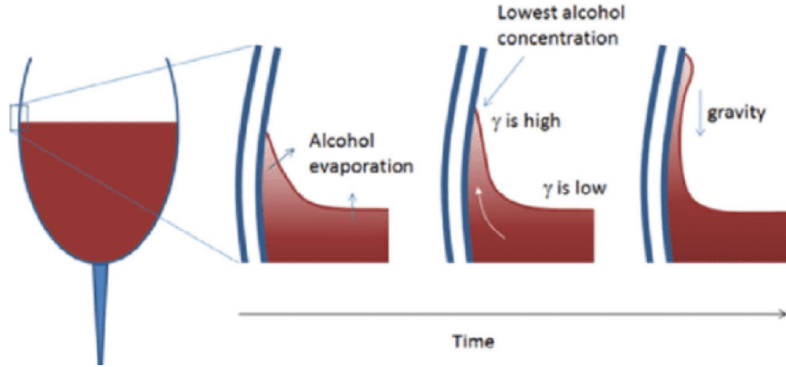


Figure 9: Mechanism of wine tears

3.2 Mechanism

Along the free surface of wine which is in contact with air, evaporation occurs. As alcohol evaporates faster than water, the concentration of alcohol decreases faster in the thin layer of the meniscus (and later also in the film), owing to its lesser surface area-to-volume ratio than of the bulk. This creates a concentration gradient, alcohol being concentrated in the bulk than at the edge. Since surface tension of alcohol is less than water, if there is less alcohol, surface tension should be more. This means the surface tension at the meniscus should be more than at the surface above bulk. Thus a surface tension gradient is created, leading to the Marangoni flow.

Meniscus, with higher surface tension, pulls the liquid surrounding it more strongly than the bulk surface. This leads to formation of a film of wine which keeps rising as evaporation keeps the concentration gradient, hence the surface tension gradient maintained. This upflow of the film is driven by the Marangoni stress until reaching the top of the film, where it accumulates in a band (ridge) of fluid. This thickens, eventually becoming gravitationally unstable, when the Marangoni stress can no longer battle the gravitational pull, thus releasing the tears of wine. These tears roll back to replenish the bulk reservoir, but with fluid that is depleted in alcohol.

This process will keep on repeating until all alcohol from the mixture is evaporated

3.3 Governing equations and formulae

3.3.1 Hydrodynamic Model

Studying a hydrodynamic model, we apply some basic principles and approximations to get some equations and boundary conditions which can help us build a model for this phenomenon. Consider the wine film of thickness δ on an impermeable, solid surface (glass) at an angle β with respect to gravity and wine to be a newtonian fluid with constant density ρ and viscosity η . The geometrical quantities, R, W, delta and h are as shown in the figure 10. Alpha is the contact angle.

Invoking quasi-steady state approximation, we can ignore curvature of glass so that film is infinitely wide along y-direction, thus taking motion of significance to happen only in the x-z plane, we get:

$$\frac{\partial v_x}{\partial x} + \frac{\partial v_z}{\partial z} = 0 \quad (1)$$

(i.e. velocity field is divergence free liquid is incompressible.)

We assume the thickness of the film to be very less than the height of the film, so we can assume lubrication approximation to hold, so pressure varies only across z-direction. Further neglecting inertia, we get:

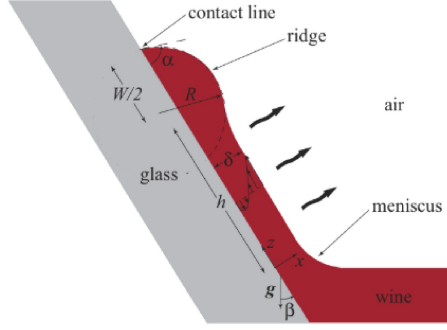


Figure 10: Schematic cross-sectional view of the evaporating film (wine) on a solid surface (glass)

$$\eta \frac{\partial^2 v_z}{\partial x^2} = p' + \rho g \cos \beta \quad (2)$$

by writing Navier-Stokes' equation along z-direction.

Taking the solid-liquid interface, i.e. $x=0$, to be impermeable and assuming no-slip, we have:

$$v_x(0, z) = 0 \quad (3)$$

$$v_z(0, z) = 0 \quad (4)$$

Evaporation flux F_{evap} is given by:

$$\rho [v_x(\delta, z) - \delta' v_z(\delta, z)] \simeq F_{evap} \quad (5)$$

A couple of useful boundary conditions are:

$$\frac{\partial v_z}{\partial x}(\delta, z) \simeq \frac{\gamma'}{\eta} \quad (6)$$

$$p(z) \simeq \gamma \delta'' \quad (7)$$

3.3.2 Finding Maximum Height of the Film (Height of the Ridge)

When equilibrium is reached, i.e. the height of the film is maximum and equal to the height of the ridge from the surface of bulk, a hydrostatic model is used as the fluid becomes momentarily static. This is a result of the fact that gravitational pull and Marangoni stress balance each other at equilibrium, hence cancelling out each other's effect. So the final height has a factor of the final interfacial tension, and not of the gradient of the interfacial tension (the marangoni stress).

By Young-Laplace Equation,

$$\rho g z = \sigma \kappa \quad (8)$$

where,

- σ is the interfacial tension at equilibrium
- κ is the curvature of the height function with respect to x

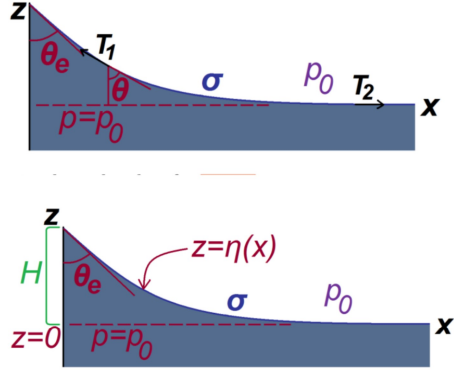


Figure 11: Shape and maximal rise height of a static meniscus

Let

$$z = \eta(x) \quad (9)$$

Using

$$\kappa = \frac{-\eta_{xx}}{(1 + \eta_x^2)^{\frac{3}{2}}} \quad (10)$$

Your LaPlace equation becomes:

$$-\rho g \eta = \sigma \nabla \cdot n = \sigma \frac{-\eta_{xx}}{(1 + \eta_x^2)^{\frac{3}{2}}} \quad (11)$$

$$\rho g \eta \eta_x = \sigma \frac{\eta \eta_{xx}}{(1 + \eta_x^2)^{\frac{3}{2}}} \quad (12)$$

$$\Rightarrow -\rho g \frac{d}{dx} \left(\frac{\eta^2}{2} \right) = \sigma \frac{d}{dx} \frac{1}{(1 + \eta_x^2)^{\frac{1}{2}}} \quad (13)$$

$$\Rightarrow \frac{\rho g \eta^2}{2\sigma} = \int_x^\infty \frac{d}{dx} \frac{1}{(1 + \eta_x^2)^{\frac{1}{2}}} dx = 1 - \frac{1}{(1 + \eta_x^2)^{\frac{1}{2}}} = 1 - \sin \theta \quad (14)$$

Therefore, we get the maximum height of the film, i.e. the height of the film at equilibrium as:

$$\eta = L_c \sqrt{2(1 - \sin \theta)} = L_c \sqrt{\frac{\sigma}{\rho g}} \quad (15)$$

3.4 Wine Tears Experiment

3.4.1 Materials Used

- A U-shaped Wine glass
- A Straight glass
- Wine : 14% (v/v) ethanol, 375 mL
 - Ethanol quantity = 52.5 mL, 41.2125 g
 - Water quantity = 322.5 mL, 322.5 g
 - Ethanol Mass fraction = 0.11331065
- Camera iPhone X
- Stand
- Thread
- A centimeter scale, LC of scale = 1mm

3.4.2 Procedure

- We first cleaned the glasses with water and dried it fully.
- Then we did the calculations for ethanol mass fraction and made a set up for the experiment. The set up consisted of a stable base to keep the glass on, a stand for the camera and adjusting the camera position to get optimum view of the glass.
- First we used the U shaped wine glass. We arbitrarily filled the glass with wine, just enough so that we can see the tears of wine.
- We then swirled the glass to wet the surface of the glass and recorded the observations.
- We noted down the height of the ridge from the meniscus by performing step (3) three times using a thread and a centimeter scale
- Steps (3), (4) and (5) were repeated for the Straight glass.

3.4.3 Expectation

We expected to see formation of a ridge and the falling of tears of wine for a long time as once the surface tension gradient is set up due to continuous evaporation, the Marangoni flow should continuously pull the thin film of wine upwards till it balances out with the gravitational force to form a ridge and then the wine tears start to fall.

3.4.4 Observations

We did observe tears of wine in both the glasses but it didn't continue for a long time as expected. There should have been a continuous flow of tears due to the continuous difference in surface tensions as evaporation took place.

- Figure (a) and (b) are of the tears of wine observed in the U shaped round glass.
- Figure (c) are the tears of wine observed in the Straight glass.

	1	2	3	Average
U -Shaped glass	8 mm	8 mm	8 mm	8 mm
Straight glass	5 mm	4-5 mm	5-6 mm	4.6 mm

Table : height of ridge observed, * For the straight glass the lower limits were considered.

Figure 12: Observation Table



(a)

Figure 13: Observation Pictures

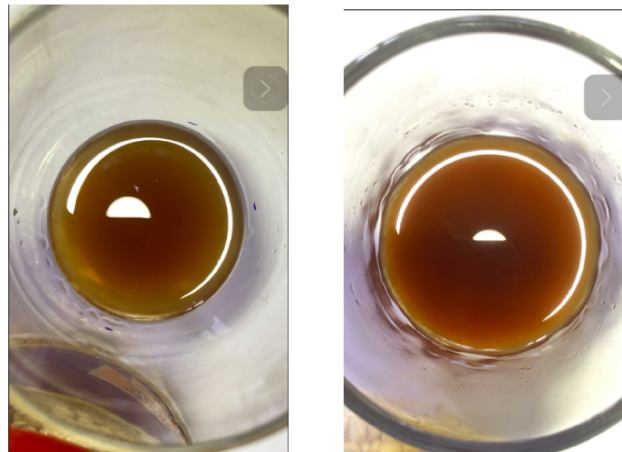


Figure 14: Observation Pictures

3.4.5 Inference

- In the paper by Venerus D C. and Simavilla D N on tears of wine, they observed the film between the meniscus and contact line had height $h \sim 10$ mm for wine which had 13% ethanol by volume i.e ethanol mass fraction ~ 0.1 and had used a V shaped glass.[1]
- We observed an average $h \sim 8$ mm for U- shaped glass and $h \sim 4.6$ mm for the Straight glass.
- The tears stopped flowing after a short time probably due to the possible errors mentioned below.

3.4.6 Possible Errors

- While in the paper by Venerus D C. and Simavilla D N , they cleaned the glass by soaking in a solution of chromic acid and hydrogen peroxide followed by rinsing with deionized water. We washed our glasses with regular tap water and let it dry. This could have contaminated the wine.
- We measured the height of the ridge using a thread and a centimeter scale which has a least count of 1 mm. We tried to minimize the errors in measurements but there could have been errors in the heights measured due to low accuracy of the equipment and experimental error.
- We performed the experiment in an open room with no controlled factors.

4 Microgravity and Spacecrafts

4.1 Introduction

A heat pipe transfers heat between two surfaces by evaporating liquid at one end and by condensing it at the other. The pipe doesn't involve any prone-to-mechanical-failure type parts, nor does it require any power so they become important technology for cooling the overall spacecraft for long missions.

But the experiments recently covered on ISS state some counterintuitive phenomena happening. In space due to microgravity the setup acts somewhat opposite. The device's performance as to how fast it can transfer heat, is limited by some mechanisms in space than on the Earth.

To dig deeper in this issue, a team of researchers imaged the interiors of a (a few centimeters long) transparent pipe which contained pentane. They heated this pipe to 523K on one end (which is the self-ignition temperature of the liquid when exposed to air). On Earth, cooling performance drops at temperatures that causes the liquid to evaporate too quickly and that hot end of the pipe to dry out. But in space, at similar temperatures something strange and opposite happens, the hot end of the pipe instead of drying out due to evaporation, was observed to be flooded by the liquid. This particular phenomenon was caused due to the competing so-called Marangoni Forces. These forces push the liquid in between regions with different surface tensions; i.e between the cold and hot ends of the device. This effect of the marangoni forces is swamped by gravity on Earth but becomes dominant in space. The temperature gradients near the heated ends may be high enough to generate significant Marangoni forces which oppose the return flow of liquid from the cold end.

4.2 Heat Pipes

These are passive heat transfer devices which find their use in high heat flux applications, where forced convection processes are not desired. So these find an important place in a microgravity environment where there is significant heat transfer due to the low Bond Number (Bo) (Bo is ratio of gravitational forces to surface tension forces.) On earth we find heat pipes in cooling systems for laptops, microprocessors etc. They work primarily via the capillary action principle. The liquid is evaporated at the heated end then it flows to the cooler end condenses there and then is returned to the heated end by some wicked or wickless design. Heat pipes are supposed to be uncomplicated designs as they have simple work-flow and the equations governing this design, operations and performance limits are well developed.

4.3 CVB Experiment

The previous problem due to the marangoni forces has to be overcome in order to make the cooling systems in spacecraft and instruments work better. So a new design of wickless pipes was proposed. The above mentioned design is the original design of a heat pipe. In order to remove certain ambiguities of the inner working of the pipe the new design proposed was specifically transparent and based on a silica spectrophotometer cell a few centimeters in length and about a centimeter squared in inner cross-sectional area. This experiment was termed as Constrained Vapor Bubble (CVB). The experiment was oriented along the y-axis of the ISS. ISS has two acceleration sensor systems that measure acceleration transients. One is the Space Acceleration Measurement System (SAMS) and other is the Microgravity Acceleration Measurement System (MAMS). The CVB setup is insensitive to transient acceleration at the SAMS frequencies (SAMS is sensitive to 0.01-400 Hz). The experiment was run by averaging over the MAMS frequencies and the average acceleration along the y-axis was observed to be $0.19\mu g$.

The working fluid was taken to be pentane which is a simple Van-der-Waals fluid which perfectly wets the fused silica surface. The Bo for these experiments was designed to be low. On the Earth it ranged from 0.8 to 27 whereas on the ISS it ranged from $1.5e-7$ to $5e-6$ over the temperature range of 273K to 423K. In this experiment the only factors to be considered were heat conduction within the walls of the heat pipe, the thermal radiation from outer surface to the surroundings at $T_{surrounding}$, and internal heat transfer

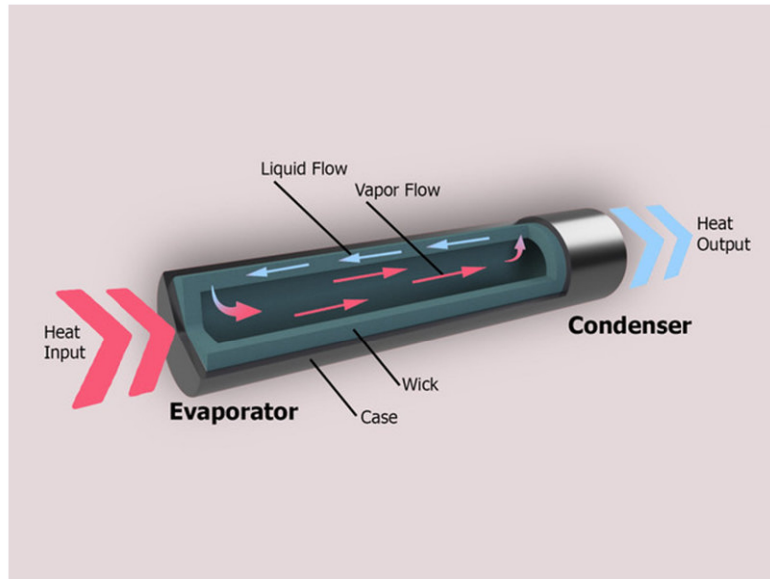


Figure 15: Heat Transfer Pipe

via evaporation or condensation to a vapor at temperature T_{vapor} . This all gets combined in a governing differential equation 16

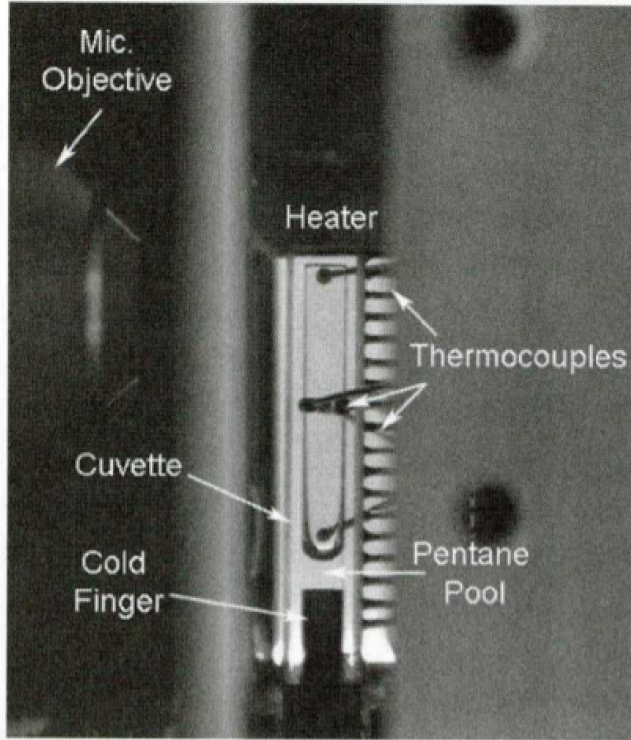


Figure 16: CVB Exp Heat Pipe

$$k_s A_s \frac{d^2 T}{dx^2} - h_i P_i (T - T_v) - \sigma \varepsilon_s P_o (T^4 - T_s^4) = 0 \quad (16)$$

k_s is the thermal conductivity of the heat pipe wall, ε_s is the emissivity of the heat pipe, P_i and P_o are the inner and the outer perimeters of the heat pipe, and A_s is the cross-sectional area of the glass portion of the heat pipe. This equation was solved with the conditions: Heated end ($x=0, T=T_h$), Cooled walls ($x=30\text{mm}, T=T_c$). and fitted to the experimentally measured temperature profiles to obtain the inside heat transfer coefficient at the heated end of the pipe.

See Fig17 The respective graphs plotted were indicative of the device reaching its limits of performance, generally assumed to be the capillary limit. However, if we look at what is actually occurring at the heated end of the device using the surveillance images of the entire device it was observed that the behavior was exactly the opposite of what was expected from the temperature profiles and what we could infer from measurements of the internal pressures. Instead of drying out the heater end, as the power input was increased, the fluid was increasingly flooded by the heated end with pentane. Over the safety limits of the experiment, it was impossible to dry out any version of our heat pipes.

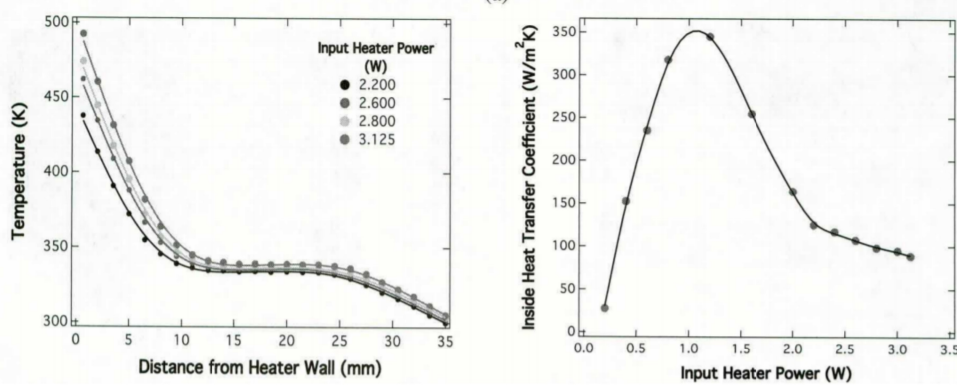


Figure 17: Temp profile and heat transfer model

At the heated end, the large temperature gradient induces a Marangoni stress at the vapor-liquid interface and this drags liquid from the heated end, where the surface tension is low, toward the cooled end, where the surface tension is higher. The actual flow field of the liquid may be much more complicated and requires further study to define. Recirculation of liquid within the thick-film Marangoni region also occurs. Though we have very thick liquid films and very high temperatures at the heated end, the boiling limit is never reached because the evaporation rate there is still too high. The device was oriented vertically with respect to gravity with the heater at the top to maintain symmetry and prevent liquid from pooling anywhere other than at the cooler. While subtle, the images clearly indicate that we have significant Marangoni effects on the ground and also the presence of a central drop, albeit appearing much closer to the cooled end. On Earth, the presence of gravity causes the capillary return flow to be weaker and the region near the heater to dry out. The result is that the central drop still forms but only further from the heater where a significant liquid film in the corner exists to support Marangoni effects and both the capillary return flow and Marangoni flow are strong enough to lead to the formation of the central drop. See Fig18

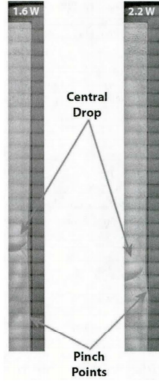


Figure 18: 30mm heat pipe image

4.4 Conclusion

By operating a transparent, wickless heat pipe in the microgravity environment of the International Space Station, it was shown that the initial limitation to heat-pipe performance in microgravity is none of the classically predicted limits. Rather than drying out or boiling at the heated end, Marangoni and capillary forces induce the exact opposite behavior, flooding the heated end with liquid that degrades performance. The temperature signatures for dry out and flooding are nearly identical, perhaps leading to the misdiagnosis in opaque heat pipes. If driven hard enough, the flooding condition must eventually break down but more experiments on the ISS will be required to unambiguously see what occurs at substantially higher temperatures, pressures, and heat inputs.

5 Coffee Ring Effect and it's suppression

5.1 Introduction

A "coffee ring" is a pattern left by a puddle of particle-laden liquid after it evaporates. The phenomenon is named for the characteristic ring-like deposit along the perimeter of a spill of coffee.

The coffee ring effect on your coffee table is not a big issue; however, its ubiquitous presence is a nuisance in many industrial applications such as in microelectronics, inkjet printing, bioassays and paints. This is because the coffee ring effect prevents formation of homogeneous residues. For example, when paints dry unwanted thicker edges can appear; printing dots can be formed as rings instead of spots; after drying, bioassays get randomly distributed, which causes difficulties in analysing them. Therefore, many technological applications require the coffee ring effect to be suppressed.

Various approaches have been developed to suppress this phenomenon, which is otherwise difficult to avoid, such as Inducing Marangoni flow(either by adding surfactants or by inducing temperature gradients), Preventing contact line pinning by using hydrophobic surfaces, Electrowetting, Using ellipsoidal particles instead of spherical etc.

Here we will specifically discuss the suppression of coffee ring effect by inducing Marangoni flow. See Fig19



Figure 19: Coffee Stains

5.2 Formation and Suppression of Coffee Rings

Required conditions for coffee ring effect to take place:

- The solvent meets the surface at a nonzero contact angle.[1]
- The contact line is pinned to its initial position.[1]
- Dispersed non-volatile solute particles should be present in the liquid which is the solvent.
- The solvent evaporates.[1]
- The particles should be spherical in shape to get a coffee ring. Ellipsoidal particles have shown to yield a uniform stain.[2]

5.2.1 According to Deegan et al[1]:

The mechanisms typically responsible for solute transport such as — surface tension gradients, solute diffusion, electrostatic, and gravity effects — are negligible in ring formation and that the phenomenon is due to

a geometrical constraint: the free surface, constrained by a pinned contact line, squeezes the fluid outward to compensate for evaporative losses.

For a liquid with a pinned contact line, evaporation takes place in the following manner[3]: See Fig20

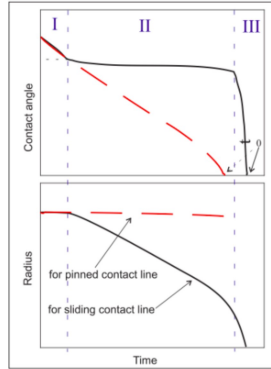


Figure 20: Evaporation of drop with pinned contact line

From the graphs we can understand that for a drop with a pinned contact line the radius of drop remains constant while the contact angle with the surface reduces continuously.

Due to evaporation the mass of fluid is not constant but decreasing. For a drop with a pinned contact line vapor leaves at a rate per unit area $J(r)$ (evaporative flux), The evaporative flux at the edges is higher than that at any other point on the liquid-air interface. The evaporative flux $J(r)$ reduces the height $h(r)$ at every point r . This means that at the perimeter, all the liquid would be removed and the drop would shrink as shown in figure a(See Fig21). But the radius of the drop cannot shrink, since its contact line is pinned. To prevent the shrinkage, liquid must flow outward from the center as shown in Figure b (See Fig21). The decrease in height causes all the solute particles to move near the solid surface and to maintain the pinned contact line the liquid along with the solute particles are pushed outwards showing forming a darker edge on evaporation, thus the coffee ring effect is seen.

To confirm their predictions they used drops of distilled water which contained charge-stabilized surfactant-free polystyrene microspheres at a starting volume fraction of $1e-4$.

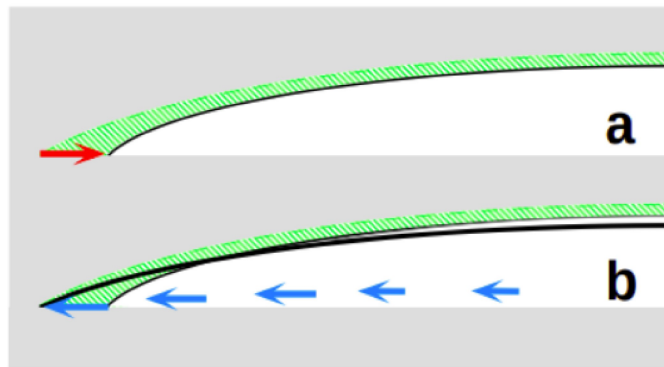


Figure 21: Increment of Evaporation in Cross Section

- Figure a shows the result of evaporation with a de-pinned contact line i.e there is no outward flow: the droplet shrinks.
- Figure b shows a fixed contact line i.e there is a compensating outward flow.

$$J(r) > \int_r^R \frac{dh(r)}{dt} dr \quad (17)$$

$$J(r) < \int_0^r \frac{dh(r)}{dt} dr \quad (18)$$

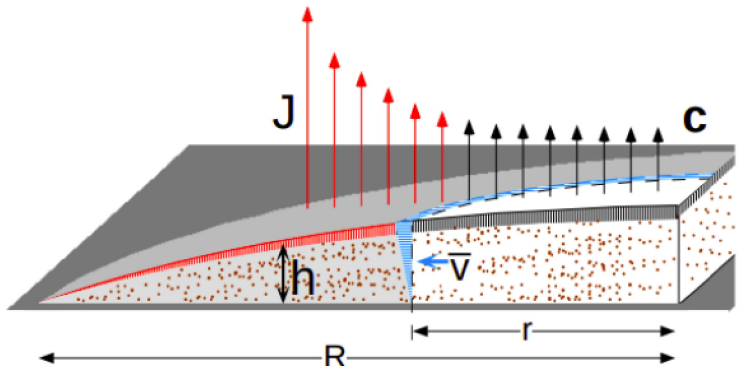


Figure 22: Flow Factors

Figure c defines quantities responsible for flow. Vapor leaves at a rate per unit area $J(r)$.

The removed liquid contracts the height $h(r)$ vertically, vacating the vertically striped region in a short time Δt . The volume of this striped region is equal to the volume removed by J . But in the shaded annular region the red-striped volume is smaller than the volume removed by $J(r)$ there (red arrows). Thus liquid flows outward to supply the deficit volume: fluid at r sweeps out the blue-striped region in time Δt .

5.2.2 According to the paper by Hua Hu and Ronald G. Larson[4]

It is shown that this explanation by Deegan et al only part of the story and that in liquids with clean droplet surfaces in which evaporation induces thermal Marangoni flows, the coffee-ring deposition is predominantly at the center rather than the edge of the droplet.

As a demonstration, they showed that fluorescent poly(methyl methacrylate) (PMMA) particles deposit preferentially near the center of a drying octane droplet.

How Marangoni flow is produced in the experiment done by Hu and Larson :

In an octane droplet a Marangoni flow is generated due to a surface-tension gradient but this flow, while theoretically expected for clean liquid surfaces, is suppressed in water droplets. Elsewhere, there is the evaporation-induced non uniform cooling along the surface of a drying droplet. The temperature at the liquid-air surface at the top center of the droplet is the lowest due to a longer thermal conduction Path than that at the edges, and the surface tension is highest there. This surface-tension gradient, finally, induces a Marangoni (i.e., surface-tension-driven) flow that carries particles that are near the free liquid surface of the droplet inward toward the top of the droplet and then plunges them downward where they can either adsorb onto the substrate near the center of the droplet or be carried along the substrate to the edge, where they are recirculated along the free surface back toward the top of the droplet.

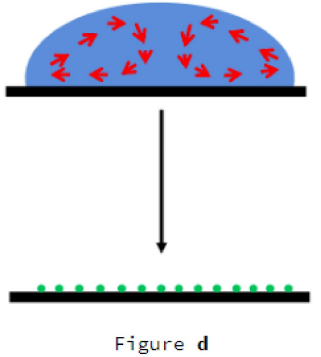


Figure 23: Figure d

For solvents such as octane and other alkanes that are not easily contaminated by surface-active agents, a strong recirculating flow is observed in the droplets implying that a large Marangoni stress is generated along the droplet surface.

5.2.3 We see the differences in the 2 papers for the following reasons :

- The 2 different results in these papers is because of the nature of liquids chosen. In the paper by Deegan et al1 the liquid under consideration is distilled water and the fluid used by Hu and Larson is octane. The Marangoni flow in the water droplet is vastly weaker than that in the latter octane droplet.[4]

Marangoni Number

The Marangoni number (Ma) is, as usually defined, the dimensionless number that compares the rate of transport due to the Marangoni flows, with the rate of transport of diffusion. The Marangoni effect is flow of a liquid due to gradients in the surface tension of the liquid. Diffusion is of whatever is creating the gradient in the surface tension.

$$Ma = \frac{\text{advection transport rate, due to the surface tension gradient}}{\text{diffusive transport rate, of source of gradient}} \quad (19)$$

A common example is surface tension gradients caused by temperature gradients. For a liquid layer of thickness L , viscosity μ and thermal diffusivity α , with a surface tension γ which changes with temperature at a rate $\partial \gamma / \partial T$, the Marangoni number can be calculated using the following formula:

$$Ma = -\frac{\partial \gamma}{\partial T} * \frac{L \Delta T}{\mu \alpha} \quad (20)$$

When Ma is small thermal diffusion dominates and there is no flow, but for large Ma, flow (convection) occurs, driven by the gradients in the surface tension. This is called Bénard-Marangoni convection.

- Hu and Larson performed the experiment by Deegan et al with double-distilled water and surfactant-free polystyrene particles to avoid introducing surfactants into the drying water droplet. However, like other authors, they found very weak Marangoni flows in water, much weaker than expected theoretically. Although the theoretical Marangoni number for a drying water droplet is around $Ma = 1000$,

experimentally they found that the Marangoni number is lower by around 100-fold, to around $Ma = 8$. They attributed this to the well-known difficulty of keeping water surfaces sufficiently clear of contaminants.[4]

- Hu and Larson argue that their conclusion of presence of Marangoni flow is only true for solvents such as octane and other alkanes that are not easily contaminated by surface-active agents, a strong recirculating flow is observed in the droplets. But in the case of water as explained by Deegan et al and also stated by Hu and Larson it is difficult to keep water surfaces sufficiently clear of contaminants.
- Thus keeping in mind the experiment and theory proposed by Hu and Larson, in everyday life we see the coffee-stain effect as explained by Deegan et al due to contamination in the solvent.

5.2.4 How is Coffee ring effect suppressed in Colloids with aqueous solvent or solvents with low Marangoni flow?

- The thermal Marangoni flow can be enhanced by elevating the temperature of the substrate resulting in an increased solute concentration near the center of the droplet . An increased temperature also increases the outwards capillary flow producing a ring as well. The result is a spot-inside-ring or an eye-like pattern.[5,6] On substrates warmer than the surrounding atmosphere, the liquid-vapour surface temperature of the droplet should decrease as going away from contact line, which generates a temperature gradient along the liquid vapour interface. The corresponding gradient in surface tension induces an inward Marangoni flow from the hot region (the drop periphery) toward the cool one (the drop apex). When the heat conductivity of the substrate compares to that of the liquid, the maximum surface temperature is not at the contact line, but close to it: a higher evaporation rate at the line causes larger cooling effects despite smaller thermal resistance. This generates a shift of maximum temperature from the line to an inner stagnation point, above which the liquid surface is entrained toward the apex of the drop.[6]

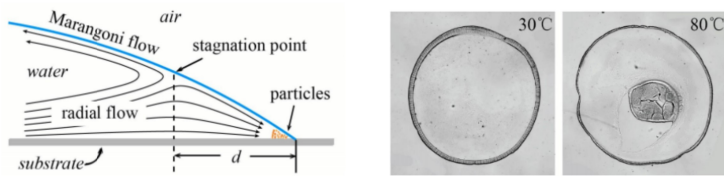


Figure 24: Figure e (i),(ii)

- The droplet surface can be locally heated using a laser beam to generate radially inward flow . In this study, an infra-red laser of wavelength $2.9 \mu\text{m}$ (as water has strong absorption at this range) was irradiated at the liquid-air interface of the droplet . When the laser exposure time was at least 60 percent of the total evaporation time of the droplet CRE was fully suppressed.[5,7]
- Marangoni flow can be induced in colloids with aqueous solvent by adding surfactants in the liquid. Surfactants decrease the surface tension of the liquid (say, water). As the liquid evaporates the concentration of the surfactants increases locally, generating strong gradients in the surface tension. The resulting Marangoni flow can overcome the capillary flow. Sodium dodecyl sulfate is an example of a commonly used surfactant.[5] Although adding chemical species to the liquid may not be desirable in some cases like in the analysis of biological samples.

5.3 Coffee Stain Experiment

5.3.1 Materials Used

- Coffee Powder
- Water
- Liquid Soap (Dettol Handwash Used)
- White Plate
- Dropper
- Measuring Cups

5.3.2 Procedure

- 2 g of coffee was mixed with 80 ml of water. The 20 ml mixture was then poured 4 cups each.
- The 4 cups were labelled and 2.5 ml, 5 ml and 10 ml of liquid soap were mixed in 3 cups respectively. Therefore we had 3 cups with various conc of liquid soap and one cup with just the coffee mixture.
- The plate was labelled and with the help of the dropper drops were placed on the plate accordingly. The dropper was thoroughly washed after dipping into a cup.
- Then the plate was left for the drops to dry without any interference.

5.3.3 Expectation

We expected to see perfect coffee rings for the drops from the cup with no liquid soap mixed. The liquid soap contains surfactants. As evaporation goes on capillary forces transfer the soap molecules to the edges which should reduce the surface tension on the coffee mix locally and there should be a surface tension gradient with the solute being pushed to the center due to Marangoni flow, thus we expected to observe a somewhat uniform stain.

5.3.4 Observation

We observed that the drops from the cup which had no liquid soap mixed had formed a perfect coffee ring at the edge as expected.

The rest of the stains show the presence of 2 rings. As the plate was not disturbed during evaporation manually nor there was appreciable wind there is an extremely low possibility of slipping of the edges. But since it didn't happen for the concentrated coffee drops, slipping must not have been the case. Plus all the stains from the soap mixed coffee mix cups show 2 rings regardless of the concentration of the concentration of liquid soap.

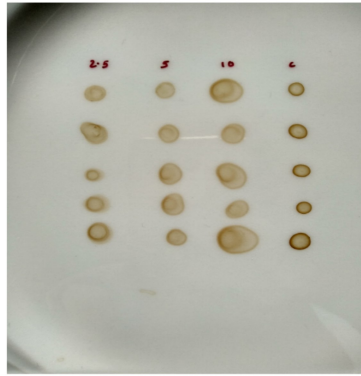


Figure 25: Coffee Drops

5.3.5 Inference

The drops from the cup which had no liquid soap mixed had formed a perfect coffee ring at the edge as expected.

The presence of 2 rings in the drops from the cups with liquid soap mixed could be explained by partial suppression of the coffee ring effect. Within the regime of experimental error it could be possible that the suppression didn't take place completely that's why we could see 2 rings instead of a somewhat uniform stain.

5.3.6 Possible Errors

- Measurement of coffee, water and liquid soap might not have been accurate.
- The water used was regular tap water instead of distilled water.
- The plate which was used as substrate was washed with water and dried thoroughly and not sterilized.
- The drops from the dropper were not of a perfect spherical cap shape.

6 A Biological Perspective

6.1 Marangoni Transport in Nature

Marangoni propulsion in nature is of particular importance to physicists, biologists, engineers and other scientists. Apart from the traditional fields such as biophysics, the concept gains popularity in unorthodox fields such as Biomimetics too due to its wide scope and applications in anthropogenic uses. The underlying principles followed in nature are the same as those explained in the earlier sections, albeit they are evolved through natural selection across evolutionary timescales.

6.1.1 Insects walking on water

Water-walking creatures have been studied for a long time (since the 19th century) and their abilities are not constrained by the effects of surface tension alone. For any creature to move, it must apply a force to its environment; the reaction force then propels it to move forward (by Newton's 3rd law). The conservation of various energies such as gravitation, kinetic (of the creature as well as the fluid) and muscular strain (chemical energy) interplay to create this motion. Considering the absence of the aerodynamic forces for the time being, the net driving force can be characterized by a complex time-dependent geometry which can be mathematically given by: See equation21

$$F = \int_s [(\rho \frac{\partial \phi}{\partial T} + \frac{\rho|u|^2}{2} - \rho gx + \sigma(\nabla \cdot n))]n - \nabla \sigma dA \quad (21)$$

The magnitude of F can simplified into its corresponding components as below: eq22

$$|F| = \rho U^2 A + \rho gh A + \rho V \frac{dU}{dt} + \mu U A + \frac{\sigma A}{w} - \nabla \sigma A \quad (22)$$

The terms in equation22 are respectively

- form drag
- buoyancy
- added mass
- viscosity
- curvature
- Marangoni

where ρ is the fluid density, u is the fluid velocity, ϕ the velocity potential, m is the mass of the body, g is the gravitational acceleration, x is the position of the body, σ is the fluid surface tension, n is the normal vector, U is the characteristic leg speed, V is the characteristic volume, A is the area, μ is the coefficient of viscosity, w is the width of the body in contact with the fluid, f is the frequency of the water-walking creature of striking the free surface with its driving leg and h is the mean leg depth below the unperturbed surface height. With such a complex array of forces at work, the computation of the hydrodynamic forces is best done numerically. Note that we make the assumption that the local curvature at the area of contact is equal to w .

Now let us understand what some of the lesser known force-types above, mean:

- The hydrostatic pressure is used when a surface is asymmetrically stricken by a body. Then a differential pressure is created across the body which in turn produces the form drag.
- When a fluid is accelerated around an accelerating body, an added mass force is observed due to the rise in the body's apparent mass.

Each of the above 6 force-types are relatively designated with distinct quantities which describe the strength of these forces with respect to each other. They are respectively called the Reynold's Number (Re), Weber Number (We), Bond number (Bo), Jesus Number (Je), Strouhal Number (St) and the Marangoni Number (Ma). They are defined as follows: See equations 23 24 29 26 27 28

$$Re = \frac{\text{inertia}}{\text{viscous}} = \frac{Uw}{\mu} \quad (23)$$

$$We = \frac{\text{inertia}}{\text{surface-tension}} = \frac{\rho w U^2}{\sigma} \quad (24)$$

$$Bo = \frac{\text{gravity}}{\text{surface-tension}} = \frac{mg}{w\sigma} \quad (25)$$

$$Je = \frac{\text{surface-tension}}{\text{buoyancy}} = \frac{1}{Bo} \quad (26)$$

$$St = \frac{\text{added-mass}}{\text{inertia}} = \frac{fw}{U} \quad (27)$$

$$Ma = \frac{\text{Marangoni}}{\text{Curvature}} = \frac{\nabla \sigma w}{\sigma} \quad (28)$$

	Buoyancy	Added mass	Inertia	Curvature	Marangoni
Surface slapping	a	Slap Stroke Recovery			
Rowing and walking			b		
Meniscus climbing			c		
Marangoni propulsion				d	

Figure 4
The dynamic classification of water walkers. Large water-walkers, such as the basilisk lizard (a), rely on a combination of form drag, added mass, and gravitational forces generated by vigorous slapping of the free surface for both weight support and propulsion. Water-walking insects and spiders rely on surface tension for weight support. Propulsive forces for most insects, such as the water strider (b), are generated by some combination of form drag and curvature forces. Others may propel themselves using capillary forces (e.g., (c) *Pyrrhulina* nymphal larvae) or Marangoni stresses (e.g., (d) *Moselyella*). Figure (a) courtesy of Hsieh & Lauder (2004).

Figure 26: Dynamic Classification of Water Walkers

Many insects including water striders have the ability to walk on water, owing to the play of form-drag and surface tension forces. Their weight is small enough not to break the surface tension of water and stay atop. The role of buoyancy in carrying the weight of the insect is negligible.

6.1.2 The Bond Number

The Bond number plays a pivotal role in this situation. The value of the Bond number dictates whether the insect can walk on water or not. If $Bo > 1$, the surface tension is capable of carrying the weight of the insect and if $Bo < 1$, the animal falls through the surface of water.

$$Bo = \frac{\text{gravity}}{\text{surface-tension}} = \frac{mg}{w\sigma} \quad (29)$$

6.1.3 Marangoni Propulsion

Now, addressing the elephant in the room, the first documented natural Marangoni propulsion study was conducted in 1905 by Billard and Bruyant when they observed a terrestrial insect (*Stenus Sp.* - Rove Beetle) faultify fall into the water and secrete a surfactant which allowed it to push itself towards the bank and up the meniscus to return back to land.

Similar studies have also been done on *Dianous Sp.* (Rove Beetle) and *Velia Sp.* (Small Water Strider).

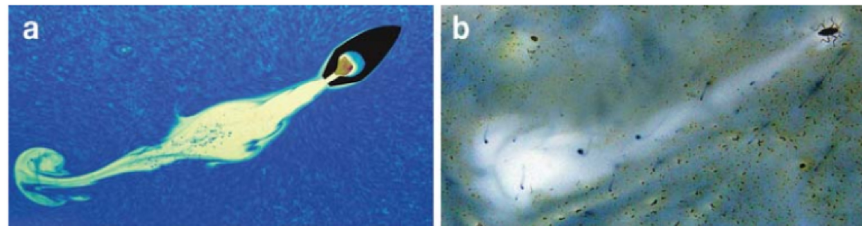


Figure 9

Marangoni propulsion for (a) a “soap boat,” and (b) *Microvelia*. The latter releases a small volume of surfactant; the resulting surface tension gradient propels it forward. In both systems, the surface divergence generated by the surfactant is evident in the clearing of dye from the free surface.

Figure 27: Marangoni Propulsion for Boat and Microvelia

Wetting arthropods mimic the propulsion mechanisms like those seen in the boat experiment but non-wetting arthropods incorporate a more composite mechanism because the bargains between kinetic and chemical energies are much more subtle. This is because the stress must be transferred through more complex intermediates such as the Water Strider’s long, thin legs onto the bulky body.

However, there are also records of the marangoni propulsion system being used for predatorial as well as fleeing purposes. This is because the propulsion provides the user a multi-fold increase in its velocity compared to its original magnitudes; which may include terrestrial, aquatic locomotions or even surfing. Biophysicists Hu and Bush are considered pioneers in regards to exploration of natural marangoni propulsion and their studies on *Microvelia sp* provides evidence to our statement by asserting that the said species can achieve a maximum propulsion speed of 17 cm/s, which is roughly twice as much as its top non-propulsion speeds through walking.

6.2 Transport of therapeutics within the lung or Marangoni enhanced pulmonary delivery strategies

Inhaled therapies have been widely used for pulmonary diseases. These provide targeted and focused action on microbes affecting the lungs rather than drugs that are injected or ingested. These inhaled therapies are easily deposited in the upper airway tracts but fail to reach the lower tracts and the alveoli. Hence, these need to be carried to the lower part of the lung. An effective method that has been used to deliver these drugs to all parts of the lung effectively is the use of Marangoni transport. The drug itself was formulated using a surfactant to propel it in the desired location or the naturally released pulmonary surfactants were used for drug delivery. The unit that carried the drug and the surfactant was formulated into microlitre drops and liquid aerosols.

6.2.1 The Airway Surface Liquid (ASL)

The airway tracts in the lungs are continually coated with a fluid. This helps in facilitating diffusion and other exchange processes across the membrane of the airway tracts. This fluid is known as the Airway

Surface Liquid (ASL) and differs in composition in the upper airway tracts, lower airway tracts and the alveoli. The ASL might also vary with different physiological conditions. The composition is as follows:

- Upper airways: the ASL has two layers:
 - Periciliary liquid (PCL): aqueous, active cilia, Brinkman fluid
 - Viscoelastic mucus layer: above PCL, contains water, glycoproteins (mucins), lipids and inorganic salts, non Newtonian fluid (flow properties are not described by a single constant value of viscosity) due to the presence of mucins.
- Lower airways: the ASL has only one layer and is composed of fewer mucin producing cells and few to no ciliated cells, Newtonian aqueous solution with a surface layer of adsorbed pulmonary surfactant.
- Alveoli: are coated with a Newtonian fluid and consist of an aqueous pulmonary surfactant.

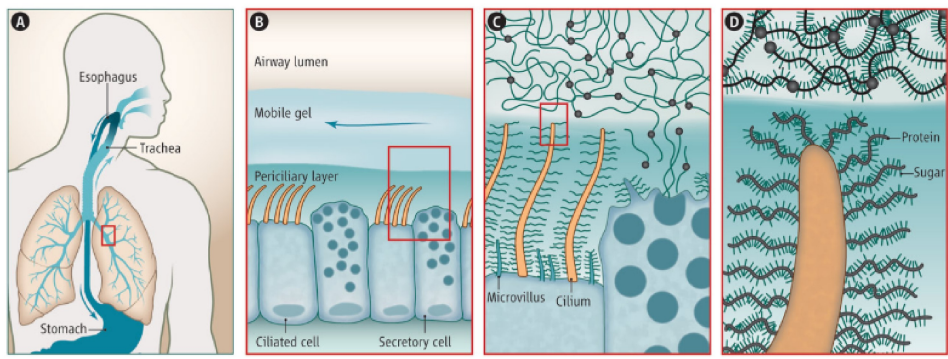


Figure 28: ASL Mechanism

6.2.2 Pulmonary surfactant

Both the lower airway tracts and the alveoli produce pulmonary surfactants but the function of this surfactant is different in both the physiological locations. In the lower airway tracts the naturally produced surfactant is composed of 90 percent phospholipids and 10 percent proteins. It serves to lower the surface tension at the air water interface and facilitates reopening of airways closed upon expiration.

The pulmonary surfactant in the alveoli helps in lowering the surface tension and thereby lowering the pressure to inflate the lungs. The alveoli expand and contract on inhalation and exhalation. This leads to change in surface tension due to change in surface energy. By lowering the surface tension, the pressure gradient across the inner and outer interface of the spherical alveoli is reduced (by Laplace's law). Hence, the pressure required to inflate the alveoli is reduced. The surface tension of the ASL is not very well understood. The reported range is very large that is 5 to 90 mN/m. But commonly found experimental values of 20-40 mN/m are generally considered.

6.2.3 Pulmonary diseases and problems in current therapy

Some common pulmonary diseases include infant respiratory distress syndrome or IRDS in which the amount of pulmonary surfactant produced is less. Hence, it becomes difficult to inflate the lungs. The current therapy available is surfactant replacement therapy but this is quite ineffective as it does not reach the inner airway tracts.

Another common disease is Cystic Fibrosis where the mucus in the pulmonary tracts becomes viscous, dry and is hence difficult to clear out. This mucus then aids in the growth of harmful bacteria. Inhaled

antibiotics kill the bacteria in the upper airway tracts but the bacteria in the lower tracts often persist and become antibiotic resistant thereby rendering the treatment ineffective.

Hence Marangoni transport is often deployed to ensure homogenous and deeper delivery of lung therapeutics. The drug therapy contained surfactants which lower the ASL surface tension locally and induce shear stresses. Hence it can be used to transport drugs across the ASL of the lung system. This had to be made sufficiently long range to reach the deeper part of the lungs.

6.2.4 System used to deliver the drug

There are 4 major components that were used to make the delivery system, namely, the surfactant, the liquid in which the surfactant is carried, the drug and the subphase onto which the drop is deposited.

A tailor made drug delivery system has to be used for each disease as the chemistry of the drug dictates the chemistry of the other components. The time evolution of these components was studied thoroughly as the sequence of events matters and has to last until the drug is delivered to the very last parts of the lung.

Efforts have been made to understand marangoni transport within the lung using systems that mimic the lung and its environment. Mucus was mimicked using thin fluid films, entangled mucin and water soluble polymer solutions. Delivery was made by microlitre (macroscopic) drops or via picolitre (microscopic) aerosol droplets.

6.2.5 Conclusion

Even though these models were performed in a controlled environment similar to that of the human body, they may fail inside an actual human body. The experimental set up however controlled does not reflect the actual human body in any way. The working of the drug might be influenced by some other biological factor present in the human body. Also, the drug delivery system may work in some people and might not in some others due to physiological differences in bodies. Also, the chemicals and surfactants used must be of appropriate concentrations and must be biologically compatible or else they might be detrimental to the health of the patient.

7 Mantle Convection

Marangoni effects can at times have surprising applications as well. In the field of Geophysics, the earth's mantle is certainly not controlled by surface tension nor marangoni effects. However, it has been found that the equations of thermal convections between the mantle and the lower lithosphere are mathematically related to those derived by the marangoni convections. In essence, it could mean that deeper exploration of the Marangoni phenomenon need not be related to traditional surfaces, but can also be correlated with pseudo surfaces that are formed dynamically within a liquid due to several properties such as differences in polarities, nano-emulsification, etc.

8 Conclusion

In this work, we have studied the Marangoni effect in different settings. From science behind the simple observations of soap boat propulsions, wine tears and coffee rings to the highly complex problems and useful applications like in biological systems and space research, Marangoni flows play an indispensable role. We started with an introduction to the Marangoni effect. We designed and performed the soap boat experiment, varying various parameters, studying their effects and noting possible shortcomings. This gave us a basic understanding of how concentration gradients cause surface tension gradients and hence Marangoni flows. Then we move to a comprehensive theoretical study of wine tears, for which we conducted our own experiment too. We observe that the wine tears differ with different concentrations of alcohol and the shape of the wine glass. Then we move onto the study of the Marangoni effect in space research, especially on how it becomes more significant in a microgravity environment. This leads to observing phenomena which we might not be able to observe in earth-like conditions and a need to adjust to them. We also see how temperature gradients come into play. We come back to earth after the previous exploration, to understand a very regularly observed phenomenon, the formation (and suppression) of coffee stains. With the help of an experiment, we derive inferences and build a theory for why the changing concentrations of liquids with different surface tensions in a water plus coffee mixture leads to formation of considerably different coffee rings. This is also attributed to the Marangoni flows which occur due to concentration as well as temperature gradient, combining the two main reasons for Marangoni effect previously studied separately. Finally, we take a look at perhaps some of the most intriguing results of this effect. We study the marangoni effect in mainly two biological systems: insect locomotion and drug delivery. Here, we introduce the concepts of Bond number to figure out when these gradient driven flows will be of a real significance. We end hereby with a detailed theoretical and experimental understanding of the Marangoni effect, understanding its importance in various scenarios, from insects to space crafts to coffee stains, compiling our shortcomings in the way, realizing how adding a small drop of soap can be matter of great significance!

9 References

9.1 For Marangoni Propulsion

Refer to 2

- Interfacial Phenomenon by Prof. John W. M. Bush, 2013
- The Marangoni Effect: How to make a soap-propelled boat, Khan Academy

9.2 For Tears of Wine

Refer to 3

- MIT OCW 18.357 Interfacial Phenomena by Prof. John W. M. Bush
- Venerus, David and Nieto Simavilla, David. (2015). Tears of wine: New insights on an old phenomenon. *Scientific Reports.* 5. 16162. 10.1038/srep16162.
- A theory for undercompressive shocks in tears of wine Yonatan Dukler, Hangjie Ji, Claudia Falcon, and Andrea L. Bertozzi

9.3 For Microgravity and Spacecrafts

Refer to 4

- <https://physics.aps.org/articles/v8/s40>
- Thermocapillary Phenomena and Performance Limitations of a Wickless Heat Pipe in Microgravity; Akshay Kundan et al 2015

9.4 For Coffee Rings and its Suppression

Refer to 5

- 1 Deegan, R. D.; Bakajin, O.; Dupont, T. F.; Huber, G.; Nagel, S. R.; Witten, T. A., Capillary flow as the cause of ring stains from dried liquid drops *Nature* 1997, Vol. 389, 827-829.
- 2 Peter J Yunker, Tim Still, Matthew A Lohr and A G Yodh, Suppression of the coffee-ring effect by shape-dependent capillary interactions, *Nature* 2011, Vol. 476, pp.308–311.
- 3 Mampallil D. Some Physics Inside Drying Droplets, *Resonance* 19(2), Feb 2014, 123-134.
- 4 Hu H, Larson RG. Marangoni effect reverses coffee-ring depositions. *J Phys Chem B* 2006;110:7090–4.
- 5 Mampallila D, Eral H B. A review on suppression and utilization of the coffee-ring effect. *Advances in Colloid and Interface Science*, Vol 252, February 2018, Pages 38-54.
- 6 Li Y, Lv C, Li Z, Quéré D, Zheng Q. From coffee rings to coffee eyes. *Soft Matter* 2015;11:4669–73.
- 7 Ta VD, Carter RM, Esenturk E, Connaughton C, Wasley TJ, Li J. et al. Dynamically controlled deposition of colloidal nanoparticle suspension in evaporating drops using laser radiation. *Soft Matter* 2016;12:4530–6.

9.5 For The Biological Perspective

Refer to 6

- Surfactant-induced Marangoni transport of lipids and therapeutics within the lung by Amy Z. Stettena, Steven V. Iasellad, Timothy E. Corcoran, Stephen Garoffa, Todd M. Przybycien and Robert D. Tilton
- Entomological fluid dynamics, John W.M Bush, Department of Mathematics, MIT
- Physics of Continuous Matter, Benny Lautrup
- Walking on Water: Biolocomotion at the interface by John W. M. Bush and David L. Hu, Department of Mathematics, MIT, 2006 Schubert, Elsevier Publication, 2015

9.6 For Mantle Convection

Refer to 7

- A model for the emergence of thermal plumes in Reileigh-Benard convection at infinite Prandtl number by C. Lemery, Y. Ricard and J. Sommeria, Laboratoire de Sciences de la Terre, ENSL, 46, allee d'Italie, 69364 Lyon Cedex 07, France, Laboratoire de Physique, ENSL, 46, allee d'Italie, 69364 Lyon Cedex 07, France, 1999-2000
- Treatise on Geophysics: Deep Earth Seismology by Barbara Romanowicz and Gerald